Revision 1

Title:

Pressure dependence of Si diffusion in γ-Fe

Authors:

[1]Noriyoshi Tsujino, [2,3]Andreea Mârza, [1]Daisuke Yamazaki

Affiliations:

[1]Institute for Planetary Materials, Okayama University, 827 Yamada, Misasa, Tottori 682-0193, Japan.

[2] Faculty of Geology and Geophysics, University of Bucharest, Bulevardul Regina Elisabeta 4-12, București 030018, Romania.

[3]Present address: Hunt Oil Company of Romania, Bucharest, Romania

Corresponding author:

Noriyoshi Tsujino: tsujino@okayama-u.ac.jp

Keywords: γ-Fe, silicon diffusion, high pressure, planetary core

Abstract

The pressure dependence of Si diffusion in γ-Fe was investigated at pressures of 5–15 GPa and temperatures of 1473–1673 K using the Kawai-type multi-anvil apparatus to estimate the rate of mass transportation for the chemical homogenization of the Earth's inner core and those of small terrestrial planets and large satellites. The obtained diffusion coefficients D were fitted to the equation $D = D_0 \exp\left(-\frac{E^* + PV^*}{RT}\right)$, where D_0 is a constant, E^* is the activation energy, P is the pressure, V^* is the activation volume, R is the gas constant and T is the absolute temperature. The least squares analysis yielded $D_0 = 10^{-1.17 \pm 0.54}$ m^2/s, $E^* = 336 \pm 16$ kJ/mol, and $V^* = 4.3 \pm 0.2$ cm^3/mol. Moreover, the pressure and temperature dependences of diffusion coefficients of Si in γ-Fe can also be expressed well using homologous temperature scaling, which is expressed as $D = D_0 exp\left(-g\frac{T_m(P)}{T}\right)$ where g is a constant, $T_m(P)$ is the melting temperature at pressure P, and D_0 and g are $10^{-1.0 \pm 0.3}$ m^2/s and 22.0 ± 0.7, respectively. The present study indicates that even for 1 billion years, the maximum diffusion length of Si under conditions in planetary and satellite cores is less than ~1.2 km. Additionally, the estimated strain of plastic deformation in the Earth's inner core, caused by the Harper–Dorn creep, reaches more than 10^3 at a stress level of 10^3–10^4 Pa, although the inner core might be slightly deformed by other mechanisms. The chemical heterogeneity of the inner core can be reduced only via plastic deformation by the Harper–Dorn creep.

Introduction

The face-centered cubic (fcc) structure of iron (γ-Fe) is stable at relatively high temperature (> 700 K) and low pressure (< 100 GPa) conditions [e.g., Komabayashi and Fei, 2010] that have been regarded as the dominant phase in the metallic cores of small terrestrial planets such as Mercury and Mars and large satellites such as the Moon and Ganymede [e.g., Tsujino et al., 2013]. The cores of terrestrial planets are primarily composed of iron alloys with certain amounts of light elements [e.g., Birch, 1952]. Because γ-Fe can contain 5–7 wt% of Si as a substitutional impurity at 10–40 GPa [e.g., Lin et al., 2002], Si can be incorporated in γ-Fe as a light element in the solid inner cores of small planets and large satellites. On Earth, a high Mg/Si ratio in the fertile mantle compared to the cosmic abundance of Si, the so-called "missing Si" [MacDonald and Knopoff, 1958], strongly suggests the presence of Si in the core. Moreover, the ratio of heavier Si isotopes ($^{29}Si/^{28}Si$) in the bulk silicate being higher than that in chondrites is interpreted to have been a result of the fractionation of metal silicate [e.g., Georg et al. 2007]. Thus, Si has been regarded as an important light element in the Earth's core and in those of small planets and satellites.

Seismological studies of the Earth's inner core have revealed that there are both spherical [e.g., Ishii and Dziewonski, 2002] and hemispherical [e.g., Tanaka and Hamaguchi, 1997] heterogeneities that could be responsible for the formation of chemical heterogeneities during the growth of the inner core. The maintenance or sustainability of these heterogeneities in the inner core on a geological time scale is

dependent on the degree of material movement directly from atomic diffusion. Another homogenizing mechanism in the inner core is mechanical stirring and mixing accompanied by convection, which is controlled by the rheological properties of Fe. It is known that under the conditions of high temperature ($> 0.6T_m$, where T_m is the melting temperature) and low stress ($< 10^{-3}\mu$, where μ is shear modulus), atomic diffusion is the rate-determining process of three dominant deformation mechanisms: the dislocation creep controlled by dislocation climb; diffusion creep; and Harper–Dorn creep [e.g., Frost and Ashby 1982]. Although the hexagonal close-packed (hcp) structure of iron (ε-Fe) would be stable at conditions in the Earth's inner core [Tateno et al., 2010], the diffusion coefficient in ε-Fe could be comparable with that in γ-Fe because both phases have the closest packed structure with, ideally, the same interatomic distances [Reaman et al., 2012]. Diffusion data of γ-Fe is applicable to discuss the Earth's inner core. Therefore, atomic diffusion in γ-Fe is key to understanding the evolution of planetary and satellite cores. The self-diffusion of Fe and diffusion of substitutional elements in γ-Fe at ambient pressure is well known [e.g., Buffington et al., 1961; Okinawa, 1982]. The diffusivity of substitutional elements in γ-Fe is not significantly different from the self-diffusivity of Fe because both atoms diffuse via point vacancies [Okinawa, 1982]. The effects of pressure on diffusivity for Au, Pd, and Re in Fe-Ni alloy, which are substitutional elements, were determined up to 10 GPa by Watson et al. [2008], and the pressure effect on inter-diffusion in Fe-Ni alloy has been reported up to 65 GPa by Reaman et al. [2012]. Nevertheless, the study of the pressure effect on the diffusivity of light elements, such as Si in γ-Fe, have

been quite limited.

In this study, we conducted diffusion experiments of Si in γ-Fe up to 1673 K and 15 GPa to determine the pressure dependence of the diffusivity of Si. Based on the diffusion data obtained, we estimated the rate of mass transportation to discuss the time scale of the chemical homogenization of the Earth's inner core and those of small terrestrial planets and large satellites.

Experimental methods

High pressure (5–15 GPa) and high temperature (1473–1673 K) experiments were conducted to determine the pressure and temperature dependence of the diffusion coefficient of Si in γ-Fe using the Kawai-type multi-anvil apparatus at the Institute for Planetary Materials, Okayama University. An assembly of cubic tungsten carbide second stage anvils (with a truncated edged length (TEL) of 7 mm) compressed the octahedral pressure medium of 5 wt% Cr_2O_3-doped MgO (with an edge length of 14 mm), in which a cylindrical graphite or TiB_2 + BN + AlN composite was used as a heater with a ZrO_2 thermal insulator. The temperature was monitored with a W97%Re3%–W75%Re25% thermocouple, and its junction was set next to the sample across the MgO disk. To observe Si diffusion in γ-Fe, pure Fe (99.99% purity, The Nilaco Corporation)—which consists of elongated grains approximately 10 μm × 10 μm × 200 μm in size and 1 wt% Si-doped Fe with grains > 200 μm in size (Rare Metallic Co., Ltd.) were used for the diffusion couple, which was surrounded by a cylindrical MgO sleeve and disks to prevent reactions with the heater and the thermocouple. The interfaces of both samples were finished by

92 careful polishing just before the experiments to minimize the formation of oxide film on them. The
93 metal couples were first compressed to the prescribed pressures at room temperature and heated to the
94 annealing temperatures (1473–1673 K) at the increasing rate of ~50 K/min. The temperature was kept
95 constant at the prescribed value within ±2 K for 2–21 h.

96 After annealing, the recovered samples which transformed from an fcc structure to the
97 body-centered cubic structure after decompression were mounted in epoxy resin and polished with
98 diamond paste (1 μm in grain size). The diffusion profiles on the polished cross section were obtained by
99 linear chemical analyses across the interface using an electron probe micro-analyzer (EPMA;
100 JEOL-8800) combined with wavelength dispersion spectroscopy (WDS) performed at the Institute for
101 Planetary Materials, Okayama University. An accelerating voltage of 15 kV and a beam current of $1.2 \times$
102 10^{-8} A were applied in conjunction with counting times of 20 s for the peak and 10 s for the background
103 signals. Pure Fe and $NiSi_2$ were used as the standards of Fe and Si, respectively, for quantitative
104 analyses.

105 **Results and Discussion**

106 The experimental conditions and diffusion coefficients of Si in γ-Fe obtained are summarized in
107 Table 1. Figures 1a and 1b show the typical secondary electron images of the cross section of the
108 recovered samples. In Figure 1c, a small number of very tiny SiO_2 particles, which might have been
109 formed by the oxidized film after the samples were polished during their preparation and/or by reaction

110 with water adsorbed on them during the experiments, were sometimes observed near the interfaces. The
111 inhibitory effect of SiO_2 particles on the diffusion process would have been negligibly small because of
112 the minor quantity of them present at the interface. As shown in Figure 1d, recovered samples show a
113 martensitic microstructure formed by back-transformation during quenching and/or decompression and
114 large domains (> 300 μm) considered to be primary γ-Fe grains formed at a high pressure and
115 temperature. The effective diffusion coefficients for polycrystalline materials consist of lattice diffusion
116 and grain boundary diffusion. Yunker and Van Orman [2007] suggested that lattice diffusion became
117 dominant when grain size was larger than ~100 μm for diffusion in fcc metals, including γ-Fe at the
118 P-T conditions similar to the present study. Therefore, lattice diffusion would be the dominant
119 mechanism in this study. Figures 2a and 2b show representative diffusion profiles, which are obviously
120 symmetrical with respect to the interface. Therefore, diffusion profiles obtained in the present study
121 were certainly formed by Si self-diffusion in γ-Fe. These profiles were analyzed using the 1D solution
122 to Fick's second law for a semi-infinite diffusion model with a constant diffusion coefficient *D*, [Crank,
123 1975] described as follows:

124 $$C(x,t) = \frac{C_0}{2} erfc\left(\frac{x}{2\sqrt{Dt}}\right) \quad (1)$$

125 where $C(x,t)$ is the Si concentration at distance x (x = 0 at the original interface) and time *t*, C_0 is
126 the initial concentration of Si in Si-doped Fe, and $erfc$ is the complementary error function.

127 Pressure and temperature effects on the diffusion coefficient can be represented by the

Arrhenius-type relation as below:

$$D = D_0 \exp\left(-\frac{H^*(P)}{RT}\right) \quad (2)$$

where D_0, R, T and $H^*(P)$ are a diffusion constant, the gas constant, the absolute temperature, and the activation enthalpy, respectively. The activation enthalpy is expressed as follows:

$$H^*(P) = E^* + PV^* \quad (3)$$

where E^*, P, and V^* are the activation energy, the pressure, and the activation volume, respectively. In equation (3), the activation enthalpy depends linearly on pressure. As shown in Figures 3a and 3b, diffusivity of Si in γ-Fe increases with increasing temperature while it decreases with increasing pressure. The least squares fit of the obtained diffusion coefficients to Eqs. (2) and (3) yielded D_0 = $10^{-1.17 \pm 0.54}$ m^2/s, E^* = 336 ± 16 kJ/mol, and V^* = 4.3 ± 0.2 cm^3/mol. In addition to the linear pressure dependency model, homologous temperature scaling, which is an Arrhenius-type plot, is frequently adopted to estimate the kinetic properties of materials [Yamazaki and Karato, 2001]. Homologous temperature scaling has also been found to provide a good description of experimental data for a broad range of metals and alloys at various conditions by Brown and Ashby [1980] and Sammis et al. [1981]. In this scaling, pressure and temperature dependences of the diffusivity are expressed through melting temperature, $T_m(P)$, at pressure, P, as below:

$$H^*(P) = gRT_m(P) \quad (4)$$

where g is a constant derived from Eq. (2). As shown in Figure 3c, D_0 and g are determined to be

146 $10^{-1.0\ \pm 0.3}$ m^2/s and 22.0 ± 0.7, respectively, by using $T_m(P)$ determined by Komabayashi and Fei
147 [2010].

148 The activation energy for Si in γ-Fe of 336 ± 16 kJ/mol at pressures of 5-15 GPa in this study is
149 larger than that at ambient pressure of 253 kJ/mol by Bergner et al. [1990]. Moreover, diffusion
150 coefficient of Si at 0 GPa extrapolated from the high pressure data in this study is slightly larger than
151 that of Si at ambient pressure determined by Bergner et al. [1990], as shown in Figure 3(a). Yamazaki
152 et al. [2004] suggested the elevated hydrogen pressure enhanced diffusion of Au in γ-Fe owing to
153 induction of vacancies. The diffusivity of Au at hydrogen pressure of 5 GPa is 2–3 times larger than it
154 is at ambient pressure. They also reported that the activation energy E^* of diffusion becomes larger
155 with the elevated hydrogen pressure. In preparation of the samples in the present study, we skipped the
156 drying process after polishing the surfaces to avoid the oxidation. In addition, hydrogen is
157 preferentially partitioned into Fe rather than silicate at a high pressure [Shibazaki et al., 2009], and the
158 water solubility of MgO surrounding the samples is very small (< 3.5 wt.ppm) [Joachim et al., 2013].
159 Therefore, some amount of hydrogen from adsorbed water may be absorbed into the samples and may
160 yield higher activation energy and diffusion coefficient measurements than those in the study by
161 Bergner et al. [1990], although such discrepancies in these values were often attributed in previous
162 studies to various experimental conditions and settings (e.g. the starting material's purity).

163 In the present study, the activation volume was determined to be 4.3 ± 0.2 cm^3/mol from the fitting

of Si diffusivity to Eqs. (2) and (3) over the experimental pressure range of 5–15 GPa. In comparison, the activation volumes of diffusivity for Au, Pd, and Re in Fe-Ni alloy at up to 10 GPa were reported to be 3–6 cm^3/mol by Watson et al. [2008], in concordance with that for Si in the present study at a similar pressure range. Additionally, the activation volumes of inter-diffusion in Fe-Ni alloy were reported to be 6 cm^3/mol at up to 4 GPa, 3.1 cm^3/mol at 0–23 GPa, and 2.6 cm^3/mol up to 63 GPa by Goldstein et al. [1965], Yunker and Van Orman [2007] and Reaman et al. [2012], respectively. Therefore, the previous studies suggest that the activation volume of inter-diffusion in Fe alloy becomes smaller with increasing pressure. In this study, the homologous temperature scaling shown in Eqs. (2) and (4) was also used to express the pressure effect on the diffusion coefficient of Si, as shown in Figure 3c. The *g*-value of 22.0 ± 0.7 in Eq. (4) in this study is also consistent with the *g*-values of 20.4 and 19.3 ± 2.7 for Fe-Ni alloy reported by Yunker and Van Orman [2007] and Reaman et al. [2012], respectively. Therefore, the homologous temperature scaling could be adapted to various pressure and temperature conditions for fcc metals. To extrapolate the Si diffusivity of the present study to pressures in the Earth's core, homologous temperature scaling is more suitable than the constant activation volume model.

Implications for planetary and satellite cores

Diffusion is one of the important mechanisms that homogenized chemical heterogeneities that occurred during the formation and growth of the inner core. Figure 4 shows the typical diffusion length

182 of Si in γ-Fe on a geologic time scale (1 billion years) under the *P-T* conditions of the cores of satellites
183 and small terrestrial planets as estimated by Tsujino et al. [2013]. Despite the fact that the core sizes of
184 these satellites and small planets (> 100 km) are large, the maximum diffusion length for 1 billion years
185 is limited to be less than 1.2 km, which is more than two orders of magnitude smaller than the cores.
186 Both γ-Fe and ε-Fe structures are close-packed, ideally with the same interatomic distances, assuming
187 that the atoms are spherical. Therefore, the diffusion coefficients in ε-Fe would be close to those in γ-Fe
188 [Reaman et al., 2012]; consequently, the diffusion coefficient in γ-Fe can be applied to the Earth's inner
189 core, which is made of ε-Fe [Tateno et al. 2010]. Assuming $T/T_m = 0.9 - 1.0$ for the Earth's core, the
190 diffusion coefficient of Si is estimated to be 3×10^{-12}–3×10^{-11} m^2/s. Therefore, the diffusion length of
191 Si is only 0.4–1.4 km for 1 billion years while the radii of the inner and innermost inner core of the Earth
192 are ~1200 km and 300–500 km [e.g., Ishii and Dziewonski, 2002], respectively. Therefore, the chemical
193 heterogeneity that formed during the growth of the inner core of terrestrial planets (including Earth) and
194 of large satellites would still be preserved only if the diffusion mechanism caused the transportation of
195 mass.

196 In general, the diffusivity of a substitutional solute atom in metal is similar to that of a solvent
197 atom because both diffuse via point defects. Diffusivity by substituting Si in Fe [Bergner et al., 1990] is
198 different from that of the self-diffusion of Fe [Buffington et al., 1961] by only half an order of
199 magnitude, as shown in Figure 3a. The pressure effect on the diffusivity of Si in γ-Fe is consistent with

200 those for Au, Pd, and Re in an Fe–Ni alloy under a similar pressure range [Watson et al., 2008].
201 Therefore, it is highly likely that the pressure and temperature dependence of Fe diffusivity in γ-Fe is
202 similar to that of Si determined in the present study. The diffusion coefficient of Fe is estimated to be 3
203 $\times 10^{-12}$ m^2/s, assuming that $T/T_m = 0.9$. Plastic deformation can mitigate the chemical heterogeneity of
204 the Earth's inner core via stirring and mixing processes accompanied with convection. At high
205 temperatures, diffusion is the rate-limiting process for the deformation of three types of mechanisms
206 [Frost and Ashby, 1982; Van Orman, 2004]. The first is dislocation creep, which is controlled by
207 dislocation climb and is represented by the following equation:

208 $$\dot{\gamma} = A\mu b \left(\frac{D}{kT}\right)\left(\frac{\sigma}{\mu}\right)^n \quad (5)$$

209 where $\dot{\gamma}$, A, μ, b, k, σ, and n are the shear strain rate, Dorn constant, shear modulus, length of
210 Burgers' vector, Boltzmann constant, stress, and stress exponent, respectively. For γ-Fe, the Dorn
211 constant and stress exponent are reported to be 4.3×10^5 and 4.5, respectively [Frost and Ashby, 1982].
212 The stress at the Earth's inner core is assumed to be 10^3–10^4 Pa [Yoshida et al., 1996]. Therefore, the
213 viscosity by dislocation creep was calculated to be 6×10^{21}–2×10^{25} Pa·s; a high stress dependency is
214 expected due to the high stress exponent. The second mechanism is diffusion creep, in which materials
215 deform as a Newtonian-viscous flow. The flow law of diffusion creep is shown as below:

216 $$\dot{\gamma} = \frac{42\Omega}{d^2}\left(\frac{D}{kT}\right)\sigma \quad (6)$$

217 where Ω is atomic volume and d is grain size of the inner core, which was estimated to be 1000–5000

m in conditions at the Earth's inner core conditions [Yamazaki et al., 2017]. Viscosity due to diffusion creep was calculated to be $1 \times 10^{26} - 2 \times 10^{27}$ Pa·s because of the large grain size. The third mechanism is Harper–Dorn creep, which becomes dominant at sufficiently low stress conditions ($< 5 \times 10^{-6}\,\mu$), although it might be artificial [e.g., Kassner et al., 2007] because it is dominant at the limited condition of very low stress. This mechanism is expressed as follows:

$$\dot{\gamma} = \rho\Omega\mu\left(\frac{D}{kT}\right)\left(\frac{\sigma}{\mu}\right) \quad (7)$$

where ρ is the dislocation density. Data for the average dislocation spacing $\rho^{-0.5}$ in Al, NaCl, and LiF lies in the vicinity of $b\mu/\sigma$ in this dislocation creep [e.g., Streb and Reppich, 1972; Blum, 1991], while the dislocation density ρ of deformed Al [Barrett et al., 1972] in the Harper–Dorn creep condition is $\sim 10^8$ /m^2 under various stress conditions. This density is consistent with the dislocation density of metal after annealing without stress. Therefore, in the Harper–Dorn creep, dislocation density is almost constant and the material deforms in a Newtonian-viscous flow. The viscosity in the Harper–Dorn creep was calculated to be 5×10^{14} Pa·s. This is the lowest viscosity in the Earth's inner core conditions among the three mechanisms, suggesting that the Harper–Dorn creep would be the dominant one. This is supported by the stress level of 10^3–10^4 Pa reported in the Earth's inner core by Yoshida et al. [1996]; a shear modulus μ = 160 GPa [Dziewonski and Anderson, 1981] is small enough for the Harper–Dorn creep.

From geophysical observation based on seismic inferences of super-rotation of the inner core

236 [Buffett, 1997], viscosity of the Earth's inner core was estimated to be $< 3 \times 10^{16}$ Pa·s, or $> 1.5 \times 10^{20}$
237 Pa·s. The viscosity in Harper–Dorn creep is consistent with the observation of $< 3 \times 10^{16}$ Pa·s. Figure 5
238 shows the variation in estimated strains as functions of stress on a geologic timescale (100 My–1000
239 My) for the three deformation mechanisms. The strain on the inner core from the Harper–Dorn creep
240 could be greater than 10^3 at a stress of 10^3–10^4 Pa, indicating that the inner core would be well-stirred
241 due to the large strain $> 10^3$. In both Harper–Dorn and dislocation creep, strain would be controlled by
242 dislocation motion and result in observed seismic velocity anisotropies [e.g., Poupinet et al., 1983]
243 through crystallographic preferred orientation (CPO). The chemical heterogeneity can be reduced by
244 stirring and subsequent diffusion and the resultant CPO can be also formed by motion of dislocation.
245 However, recent studies suggested that Harper–Dorn creep might be artificial [e.g., Kassner et al., 2007].
246 If the Harper–Dorn creep was not realized, dislocation creep would preferentially dominate deformation
247 in the Earth's inner core. The viscosity of dislocation creep was also consistent with the geophysical
248 observation of $> 1.5 \times 10^{20}$ Pa·s [Buffett, 1997], and the inner core would be deformed slightly, as
249 shown in Figure 5. Using dislocation creep CPO could not be developed, owing to the small strain level
250 [Nishihara et al., 2019], to explain the seismic anisotropy in the inner core. Therefore, the conclusion is
251 that chemical heterogeneity can only be reduced via plastic deformation by the Harper–Dorn creep.
252
253

Acknowledgements

We appreciate Takashi Yoshino, Eiji Ito, Fang Xu, and HACTO group members for their help in conducting diffusion experiments and for their advice during discussions. Official review by Jim Van Orman and one anonymous reviewer improved the quality of the manuscript. This work was supported by Grant-in-Aid for Scientific Research (B) (18H01314) and Grant-in-Aid for Scientific Research on Innovative Areas (18H04369) to NT. It was also supported by the Internship Program (MISIP14) of the Institute for Planetary Materials, Okayama University.

References

Barrett, C.R., Muehleisen, E.C., and Nix, W.D. (1972) High temperature-low stress creep of Al and Al + 0.5% Fe. Materials Science and Engineering: A, 10, 33–41.

Buffington, F.S., Hirano, K., and Cohen, M. (1961) Self diffusion in iron. Acta Metallurgica, 9, 434-439.

Bergner, D., Khaddour, Y., and Lörx, S. (1990) Diffusion of Si in bcc- and fcc-Fe. Defect and Diffusion Forum, 66-69, 1407-1412.

Birch, F. (1952) Elasticity and constitution of the Earth's interior. Journal of Geophysical Research, 57, 227–286.

Blum, W. (1991) Creep of aluminum and aluminum alloys. In: Langdon, T.G., Merchant, H.D., Morris, J.G., Zaidi, M.A. (Eds.), Creep of Aluminum and Aluminum Alloys, The Minerals. Metals and Materials Society, Warrendale, PA, pp. 181–209.

Brown, A.M., and Ashby, M.F. (1980) Correlations for diffusion constants, Acta Metallurgica, 28, 1085–1101

Buffett, B.A., (1997) Geodynamic estimates of the viscosity of the Earth's inner core. Nature, 388, 571–573.

Crank, J. (1975) Mathematics of diffusion. Oxford University Press, New York.

Dziewonski, A.M., and Anderson, D.L. (1981) Preliminary reference Earth model. Physics of the Earth and Planetary Interiors, 25, 297–356.

Frost, H. J., and Ashby, M. F. (1982) Deformation-Mechanism Maps: The Plasticity and Creep of Metals and Ceramics, Pergamon, Oxford, U. K.

Georg, R.B., Halliday, A.N., Schauble, E.A., and Reynolds, B.C. (2007) Silicon in the Earth's core. Nature, 447, 1102–1106.

Goldstein, J.J., Hanneman, R.E., and Ogilvie, R.G., (1965) Diffusion in the Fe–Ni system at 1 atm and 40 kbar pressure. Transactions of the Metallurgical society of AIME, 233, 812–820.

Ishii, M., and Dziewonski, A. M. (2002) The innermost inner core of the Earth: Evidence for a change in anisotropic behavior at the radius of about 300 km, Proceedings of the National Academy of Sciences of the United States of America, 99, 14,026–14,030.

Joachim B., Wohlers. A., Norberg, N., Garde´s E., Petrishcheva, E., and Abart, R. (2013) Diffusion and solubility of hydrogen and water in periclase. Physics and Chemistry of Minerals, 40, 19-27.

Kassner, M.E., Kumar, P., and Blum, W. (2007) Harper–Dorn creep. International Journal of Plasticity, 23, 980–1000.

Komabayashi, T., and Fei, Y.W. (2010) Internally consistent thermodynamic database for iron to the Earth's core conditions. Journal of Geophysical Research–Solid Earth, 115, B03202.

295 Lin, J.F., Heins, D.L., Campbell, A.J., Devine, J.M., and Shen, G. (2002) Iron-silivin alloy in Earth's
296 core?. Science, 295, 313-315.
297 MacDonald, G.J.F., and Knopoff, L. (1958) On the chemical composition of the outer core. Geophysical
298 Journal of the Royal Astronomical Society, 1, 284–297.
299 Nishihara, Y., Ohuchi, T., Kawasoe, T., Seto, Y., Maruyama, G., Higo, Y., Funakoshi, K., Tange, Y.,
300 and Irifune, T. (2019) Deformation-induced crystallographic-preferred-orientation of hcp-iron: An
301 experimental study using a deformation-DIA apparatus, Earth and Planetary Science Letters, 490,
302 151-160.
303 Oikawa, H. (1982) Lattice diffusion in iron – A review. Tetsu-to-Hagané, 68,1489–1497.
304 Poupinet, G., Pillet R., and A. Souriau A. (1983) Possible heterogeneity of the Earth's core deduced
305 from PKIKP travel times, Nature, 305, 204-206.
306 Reaman, M.D., Colijn, H.O., Yang, F., Hauser, A.J., and Panero, W.R. (2012) Interdiffusion of Earth's
307 core materials to 65 GPa and 2200 K. Earth and Planetary Science Letters, 349-350, 8-14.
308 Sammis, C.G., Smith, J.C., and Schubert. G. (1981) A critical assessment of estimation methods for
309 activation volume, Journal of Geophysical Research, 86, 10707–10718.
310 Shibazaki, Y., Ohtani, E., Terasaki, H., Suzuki, A., and Funakoshi, K. (2009) Hydrogen partitioning
311 between iron and ringwoodite: Implications for water transport into the Martian core. Earth and
312 Planetary Science Letters, 287, 463-470.
313 Streb, G., and Reppich, B. (1972) Steady state deformation and dislocation structure of pure and
314 Mg-doped LiF single crystals. Physica Status Solidi A, 16, 493-505.
315 Tanaka S, and Hamaguchi H. (1997) Degree one heterogeneity and hemispherical variation of
316 anisotropy in the inner core from PKP(BC)-PKP(DF) times. Journal of Geophysical Research,
317 102(B2):2925–38.
318 Tateno S, Hirose K, Ohishi Y, and Tatsumi Y. (2010) The structure of iron in Earth's inner core. Science,
319 330:359–61.
320 Tsujino, N., Nishihara, Y., Nakajima, Y., Takahashi, E., Funakoshi, K, and Higo, Y. (2013) Equation of
321 state of γ-Fe: Reference density for planetary cores. Earth and Planetary Science Letters. 375,
322 244-253.
323 Van Orman, J.A. (2004) On the viscosity and creep mechanism of Earth's inner core. Geophysical
324 Research Letters, 31, L20606.
325 Watson, H.C., Watson, E.B., and Fei, T.W. (2008) Diffusion of Au, Pd, Re and P in FeNi alloys at high
326 pressure. Geochimica et Cosmochimica Acta, 72, 3550-3561.
327 Yamazaki, D., and S. Karato (2001), Some mineral physics constraints on the rheology and geothermal
328 structure of Earth's lower mantle, American Mineralogist, 86, 385–391.
329 Yamazaki, Y., Iijima, Y., and Okada, M. (2004) Enhanced diffusion of Au in c-Fe by vacancies induced

under elevated hydrogen pressure. Acta Materialia, 52, 1247-1254.
Yamazaki, D., Tsujino, N., Yoneda, A., Ito, E., Yoshino. T., Tange, Y., and Higo, Y. (2017) Grain growth of ε-iron: Implications to grain size and its evolution in the Earth's inner core. Earth and Planetary Science Letters, 459, 238-243.
Yoshida, S., I. Sumita, and M. Kumazawa (1996) Growth model of the inner core coupled with outer core dynamics and the resultant elastic anisotropy. Journal of Geophysical Research, 101, 28085-28103.
Yunker, M.L., Van Orman, J.A. (2007) Interdiffusion of solid iron and nickel at high pressure. Earth and Planetary Science Letters, 254, 203–213.

339 Figure captions

340 Figure 1. Secondary electron images of the whole recovered samples in (a) 1k2788 (1473 K, 5 GPa, 21
341 h) and (b) 1k2845 (1673 K, 10 GPa, 2 h). The upper and lower parts are 1 wt% Si-doped Fe and pure Fe,
342 respectively. (c) Expanded secondary electron image of the black square in (a). Tiny particles of SiO_2
343 near the interface between 1 wt% Si-doped Fe and pure Fe. (d) Backscattered electron image of the
344 etched recovered sample of (a) in 1k2788 (1473 K, 5 GPa, 21 h). The domain size, which represents the
345 grain size of γ-Fe at high pressure and temperature, is much larger than 300 μm.

346

347 Figure 2. The typical diffusion profiles of Si measured by linear chemical analyses using an electron
348 probe micro-analyzer in (a) 1k2788 (1473 K, 5 GPa, 21 h) and (b) 1k2845 (1673 K, 10 GPa, 2 h). Gray
349 symbols and black lines show the measurement data of normalized Si concentrations and the lines fitted
350 using Eq. (1), respectively.

351

352 Figure 3. Temperature and pressure dependence of the Si self-diffusion coefficient. The constant
353 pressure dependency model is assumed in (a) and (b) and homologous temperature scaling is applied in
354 (c). Fitting is shown by the solid lines. Red, green, and blue symbols represent diffusion data at 1673 K,
355 1573 K and 1473 K, respectively. Square, circle, and diamond symbols indicate diffusion data at 5 GPa,
356 10 GPa and 15 GPa, respectively. The broken and dotted lines in (a) show Si self-diffusion [Bergner et

357 al., 1990] and Fe self-diffusion [Buffington et al., 1961], respectively, in γ-Fe at atmospheric pressure.

358

359 Figure 4. Estimated diffusion length of Si in γ-Fe on a timescale of 1000 My for the inner cores of
360 satellites and small planets, with conditions summarized by Tsujino et al. (2013). Purple, orange, green,
361 and blue regions show the diffusion lengths for Ganymede, the Moon, Mercury, and Mars, respectively.

362

363 Figure 5. Estimated strains in the Earth's inner core for dislocation creep controlled by dislocation climb
364 (pink), diffusion creep (light blue), and the Harper–Dorn creep (green) as a function of stress on a
365 geologic timescale (100 My–1000 My). The gray area indicates the typical stress of the Earth's inner
366 core [Yoshida et al., 1996].

Table 1. Experimental conditions and the obtained diffusion coefficients of Si in γ-Fe.

Run No.	Pressure (GPa)	Temperature (K)	Duration (h)	log D_{Si} (m^2/s)
1K2788	5	1473	21	-13.86(1)
1K2794	5	1573	4	-13.01(2)
1K2786	5	1673	3	-12.36(1)
1K2846	10	1573	10	-13.83(2)
1K2845	10	1673	2	-13.06(1)
1K2852	15	1673	10	-13.64(2)

Figure 1

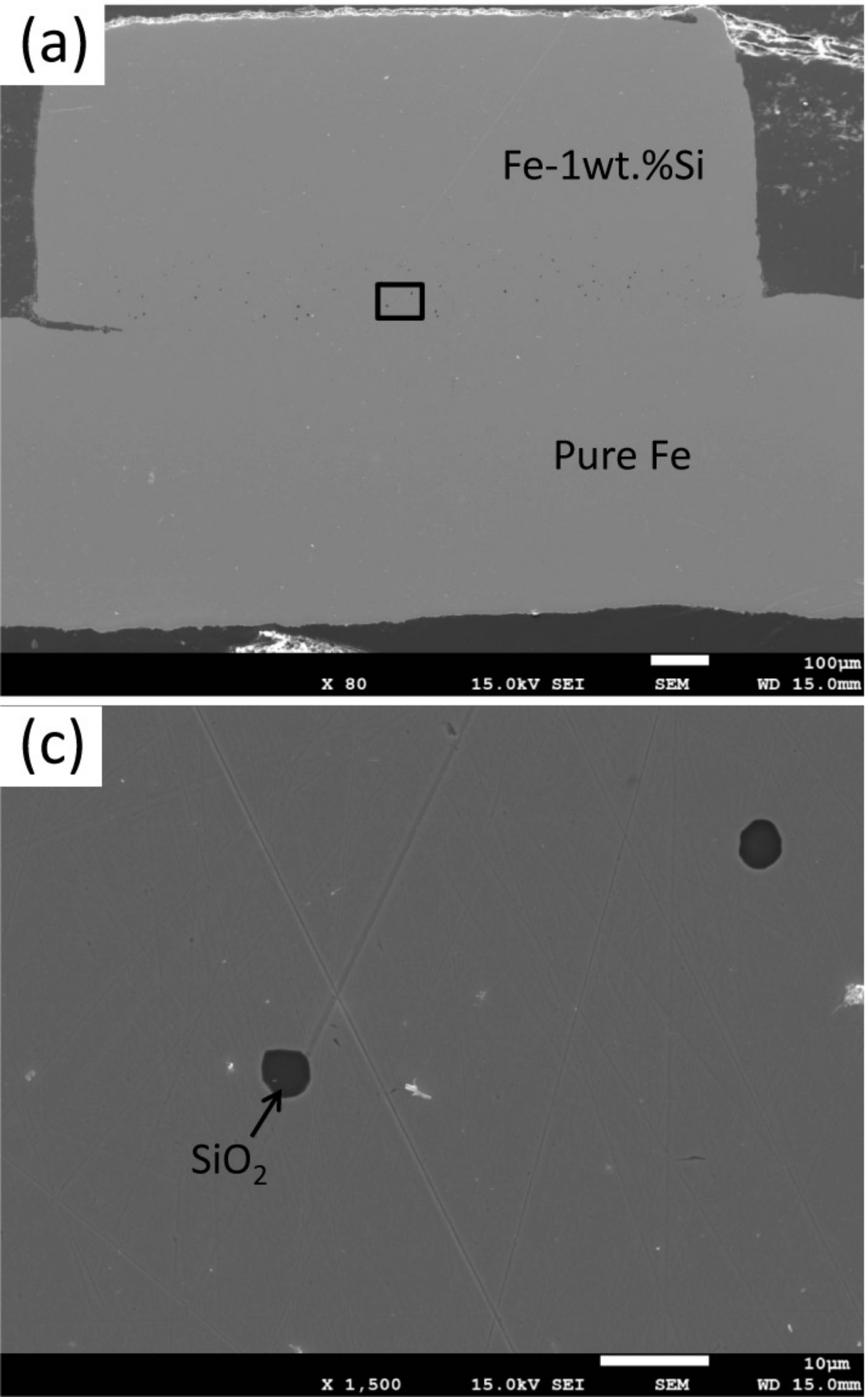
(a)
Fe-1wt.%Si
Pure Fe
100µm
X 80 15.0kV SEI SEM WD 15.0mm
(b)
Fe-1wt.%Si
Pure Fe
100µm
X 80 15.0kV SEI SEM WD 15.0mm
(c)
SiO2
10µm
X 1,500 15.0kV SEI SEM WD 15.0mm
(d)
100µm
X 200 15.0kV COMPO SEM WD 15.0mm

Figure 2

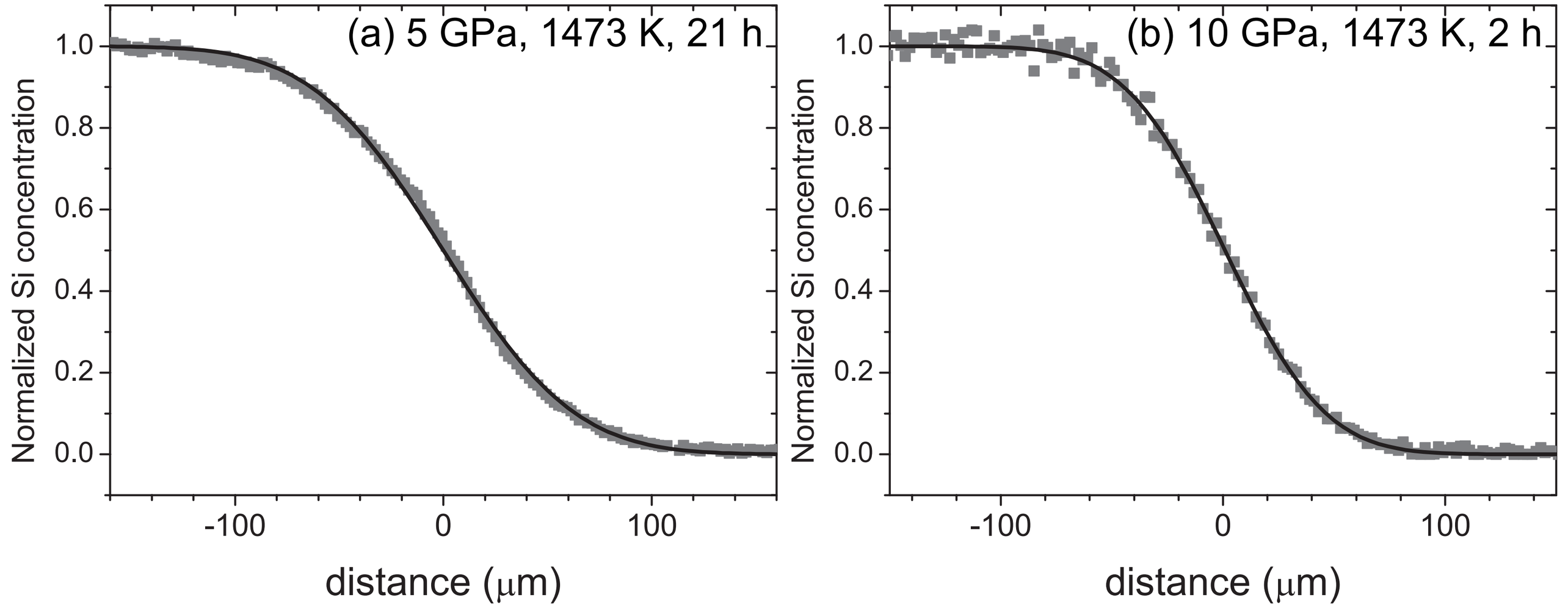
(a) 5 GPa, 1473 K, 21 h
(b) 10 GPa, 1473 K, 2 h
Normalized Si concentration
1.0
0.8
0.6
0.4
0.2
0.0
-100
0
100
distance (μm)

Figure 3

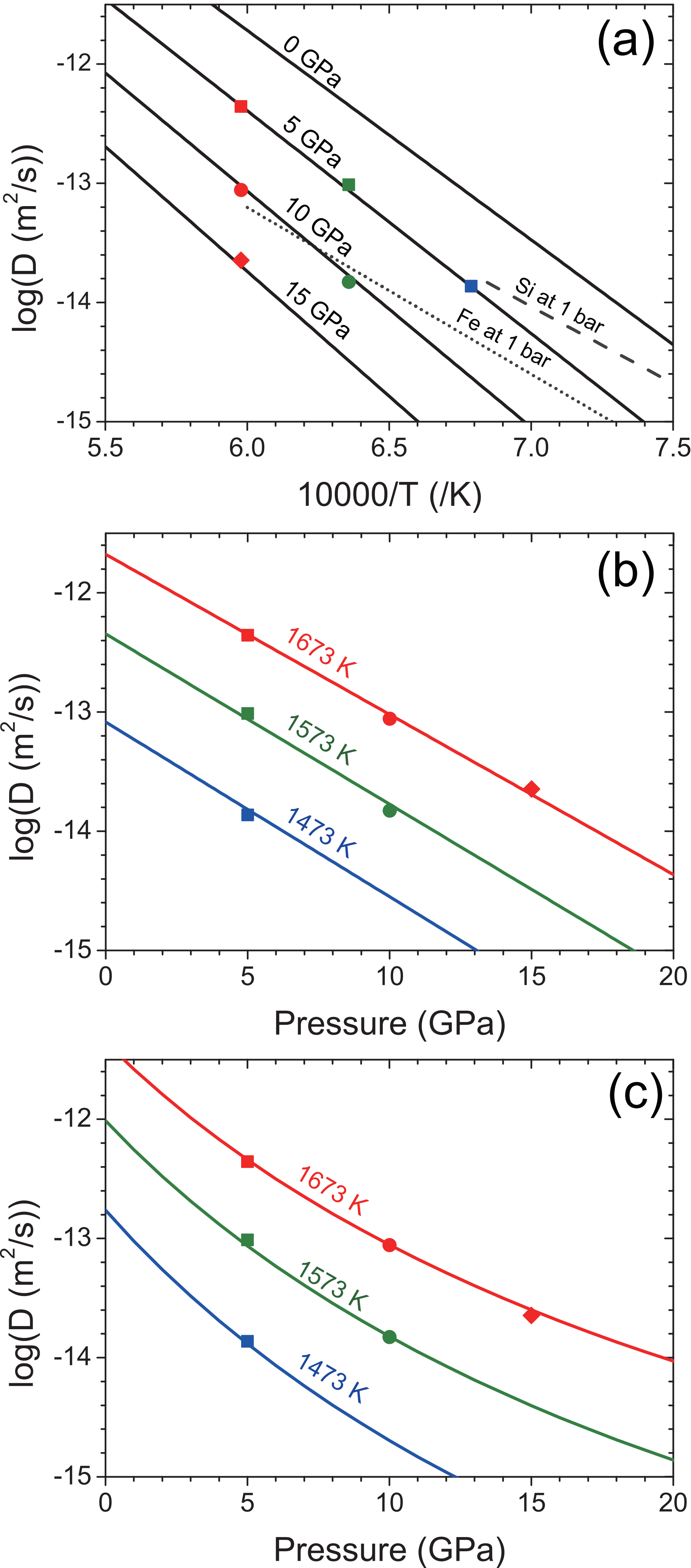
(a)
0 GPa
5 GPa
10 GPa
15 GPa
Si at 1 bar
Fe at 1 bar
log(D (m²/s))
-12
-13
-14
-15
5.5
6.0
6.5
7.0
7.5
(b)
10000/T (/K)
1673 K
1573 K
1473 K
0
5
10
15
20
(c)
Pressure (GPa)

Figure 4

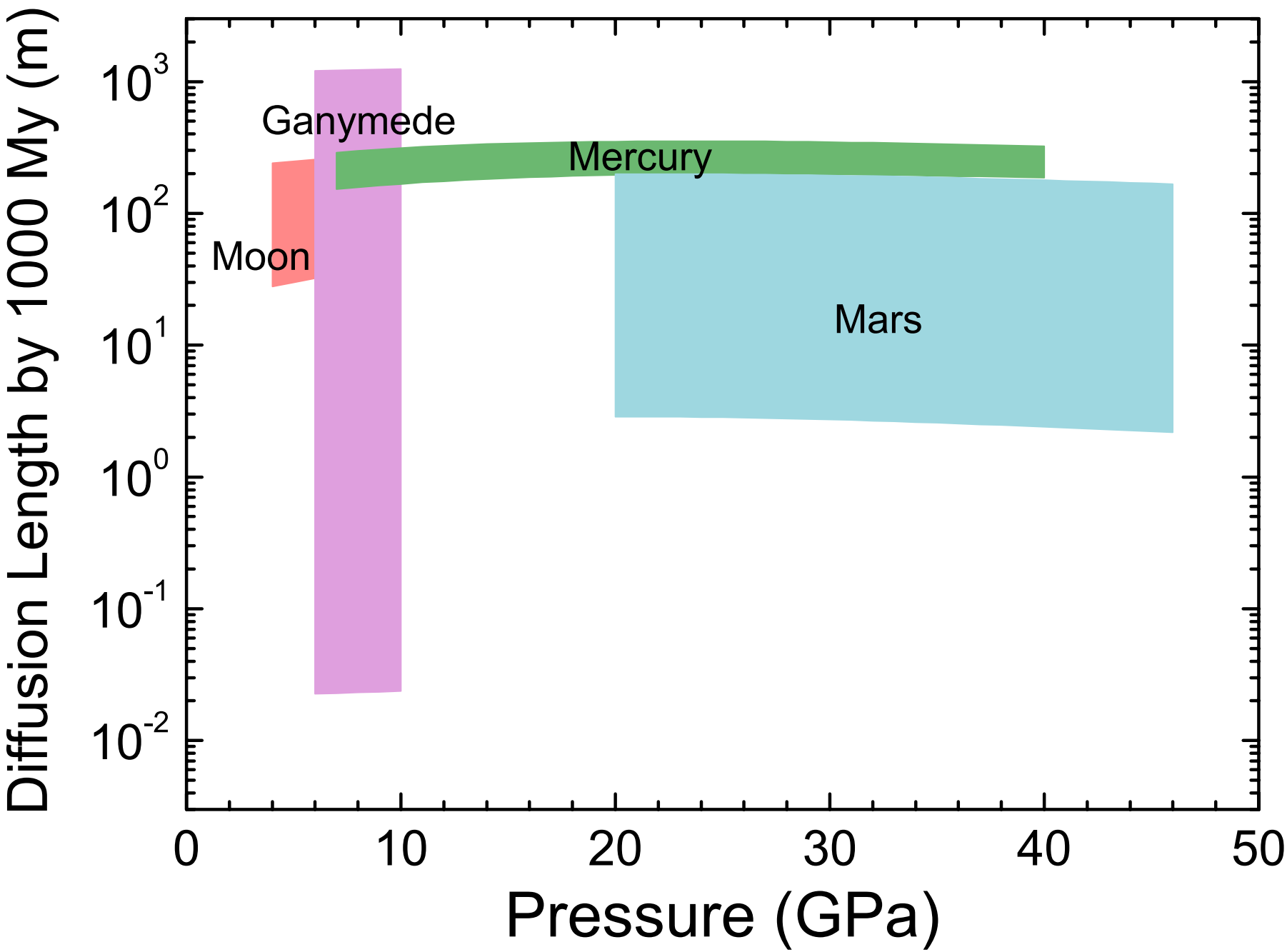
Diffusion Length by 1000 My (m)
10^{3}
10^{2}
10^{1}
10^{0}
10^{-1}
10^{-2}
Ganymede
Mercury
Moon
Mars
0
10
20
30
40
50
Pressure (GPa)

Figure 5

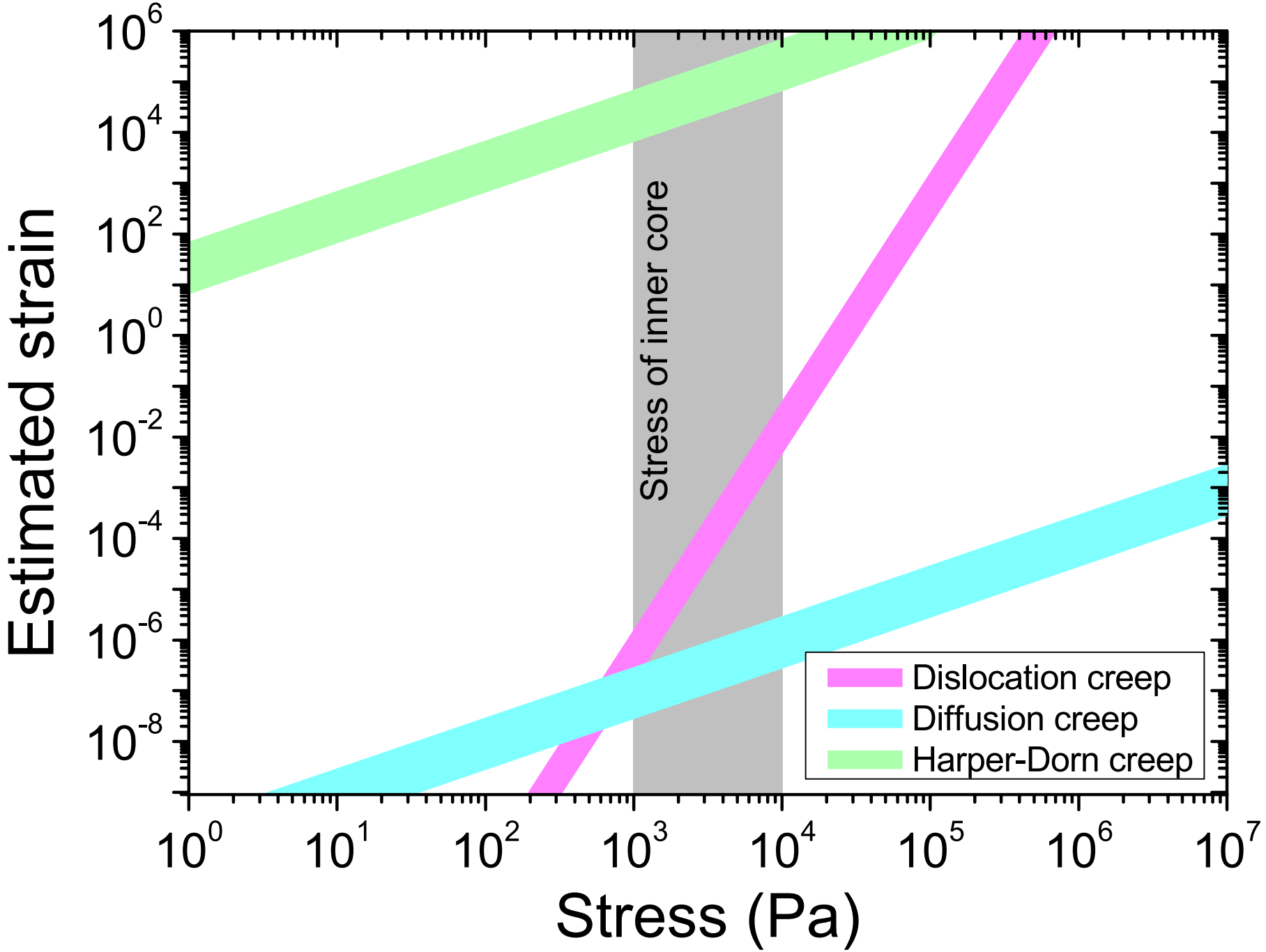
Estimated strain
10^{6}
10^{4}
10^{2}
10^{0}
10^{-2}
10^{-4}
10^{-6}
10^{-8}
Stress of inner core
Dislocation creep
Diffusion creep
Harper-Dorn creep
10^{0}
10^{1}
10^{2}
10^{3}
10^{4}
10^{5}
10^{6}
10^{7}
Stress (Pa)